Connected Cooperative Ecodriving System Considering Human Driver Error

Xuewei Qi, *Member, IEEE*, Peng Wang, *Member, IEEE*, Guoyuan Wu, *Senior Member, IEEE*, Kanok Boriboonsomsin, *Member, IEEE*, and Matthew J. Barth, *Fellow, IEEE*

***Abstract*— In recent years, eco-friendly driving or ecodriving technologies are being developed to assist human drivers to achieve maximum fuel/energy efficiency in different driving conditions. Enhanced by V2X wireless communications, connected ecodriving is expected to be very promising in reducing transportation-related fossil fuel consumption as well as pollutant emissions. Besides, the deployment of electric vehicles (EVs) also has great potential in reducing greenhouse gas emissions due to the use of batteries as the sole energy source. Although recent research shows that significant energy savings can be achieved with the aid of ecodriving systems in real-world driving, there have been very few research efforts that consider human driver error, especially for electric vehicle (EV) driving. In this paper, a connected cooperative ecodriving system for energy-efficient driving that considers human driver error is designed and evaluated with an EV energy consumption model. Real-world driving data were collected and used to evaluate system performance in terms of energy consumption. The simulation and numerical analysis shows that an average of 12% energy savings can be achieved by the proposed system that considers human driver error comparing with the conventional ecodriving system without considering driver error.**

***Index Terms*— Intelligent vehicles, advanced driver assistance systems, electric vehicles, ecodriving.**

NOMENCLATURE

d	distance of vehicle to intersection
T	desired time to arrival at the intersection
$v(t)$	vehicle speed at time step t
$v_r(t)$	reference speed of the vehicle at time t
$x(t)$	the vehicle's position at time t
v_M	upper bound of allowed vehicle speed
v_m	lower bound of allowed vehicle speed
a_M	bound of vehicle acceleration
d_M	bound of vehicle deceleration
du_M	upper bound of jerk
$u_f(t)$	actual acceleration/deceleration of vehicle
$u(t)$	reference acceleration/deceleration suggested by the driving assistance system
w	human error
C_D	the drag coefficient of the vehicle
ρ_a	the air density
A_v	the frontal area of the vehicle
M	the vehicle mass
θ	the road gradient
g	the acceleration of gravity
μ	the rolling friction coefficient
N_e	number of discretized error states
T_e	transition matrix of Markov chain
τ_{ij}	transition probability from state i to state j
l	time horizon of the stochastic model predictive control
p_s	probability of error occurrence
N_e	total number of scenario trees
N_{mc}	number of scenarios generated by Monte Carlo method
t_0	initial time
k	time step in stochastic model predictive control

Manuscript received December 23, 2016; revised May 11, 2017, September 25, 2017, and February 7, 2018; accepted May 6, 2018. Date of publication June 27, 2018; date of current version August 1, 2018. The Associate Editor for this paper was F. Bellotti. *(Corresponding author: Xuewei Qi.)*

X. Qi is with the Department of Electrical and Computer Engineering, University of California at Riverside, Riverside, CA 92507 USA (e-mail: qixuewei@gmail.com).

P. Wang and M. J. Barth are with the Department of Electrical Engineering, University of California at Riverside, Riverside, CA 92507 USA.

G. Wu and K. Boriboonsomsin are with the Center for Environmental Research and Technology, College of Engineering, University of California at Riverside, Riverside, CA 92507 USA.

Color versions of one or more of the figures in this paper are available online at http://ieeexplore.ieee.org.

Digital Object Identifier 10.1109/TITS.2018.2845799

I. INTRODUCTION

AIR pollution and climate change impacts associated with the use of fossil fuels in transportation have continued to attract public attention. Reducing transportation-related energy consumption as well as criteria pollutant and greenhouse gas (GHG) emissions has been one of the goals of public agencies and research institutes for years. In 2014, the total energy consumed by the transportation sector in the United States was as high as 24.90 Quadrillion BTU (British Thermal Unit) [1]. The U.S. Environmental Protection Agency (EPA) reported that nearly 27% GHG emissions resulted from fossil fuel combustion for transportation activities in 2014 [2]. Therefore, many researchers are motivated to search for different ways to reduce transportation-related fuel consumption and emissions from different perspectives [3]–[8]., such as, 1) building more environmentally friendly vehicles, which includes but is not limited to creating alternative fuel vehicles (AFVs), e.g., electric vehicles (EVs); 2) taking advantage of transportation infrastructure, for example, reducing traffic congestion or unnecessary stop-and-go behaviors at signalized intersections in arterials by using vehicle-to-infrastructure (V2I) wireless communication;

and 3) analyzing the impact of human driving behavior on vehicle energy consumption. For example, the unnecessarily aggressive acceleration and decelerations could be reduced to avoid additional energy consumption by training the drivers to have good driving habits through the ecodriving training programs [8].

Transportation electrification is one of the promising ways to significantly reduce fossil fuel consumption and emissions from the transportation sector. However, the mass adoption of EVs has been impeded by limited availability of charging infrastructure, long charging time, and limited travel range per charge. These can cause driver's concern which is called "range anxiety" [9]. There have been efforts to overcome these barriers by advancing battery technology [10] and investing in electric charging infrastructure [11]. However, very few efforts so far have been focused on improving the energy efficiency of EVs through vehicle connectivity and automation. Furthermore, the dynamic interactions between vehicle, infrastructure, and human driver and their aggregated energy impact on the energy efficiency of EV driving is not well investigated.

To fill the research gap, a driver-in-the-loop connected ecodriving system for energy-efficient driving that considers human driver error is designed under a driver-vehicle-infrastructure cooperation framework. The proposed system is evaluated with electric vehicle energy consumption model and compared with a conventional ecodriving system that does not consider human driver error. The designed system is capable of estimating the human driver error and making adjustment to mitigate the negative impact of such error on system effectiveness in order to achieve the maximum energy efficiency benefit. Real-world driving data were collected and used to evaluate system performance in terms of energy consumption. The major contribution of this study is its effort to advance the state-of-the-art of ecodriving by considering the human errors for EV driving. It is the first-of-its-kind connected cooperative ecodriving system considering human driver error that is evaluated with real-world EV driving data.

II. Background & Related Works

A. Connected Ecodriving Technology

In recent years, a significant amount of effort has been made worldwide in developing energy/environment-focused connected vehicle (CV) applications through various research programs, for instance, the European Union (EU)'s eCoMove [12] and Compass4D [13] programs and the United States' AERIS (Applications for the Environment: Real-Time Information Synthesis) program [14]. Among all the CV applications developed under the AERIS program, the Eco-Approach and Departure (EAD) at signalized intersections application is furthest along and has shown great promise in terms of reducing fuel consumption and emissions [15]. Just like many other CV applications that involve determining optimal speed profiles for vehicles traveling within the urban transportation network (e.g., [16]–[20]), the EAD application utilizes signal phase and timing (SPaT) information from the upcoming traffic signal to determine a speed profile that minimizes fuel consumption and emissions when approaching and departing the signalized intersection. The speed profile is then conveyed to the driver through a driver-vehicle interface.

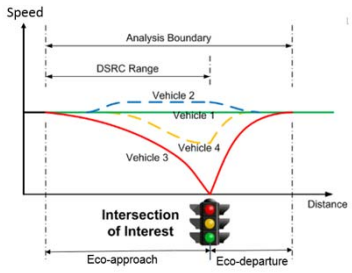

Fig. 1. Illustration of different vehicle trajectories traveling across a signalized intersection.

Basically, there are four different "*passing scenarios*" when a vehicle travels through an isolated signalized intersection without the interaction with other traffic. The speed profiles of these four scenarios are shown in Fig.1. All these speed profiles have the same initial and final speeds and cover the same distance (i.e., the analysis boundary). Each passing scenario can be described as follows:

- Scenario 1 (cruise): The vehicle cruises through the intersection at a constant speed (green solid line);
- Scenario 2 (speed up): The vehicle speeds up (within the speed limit) to pass through the intersection and then slows down to the initial speed after the intersection (blue dashed line);
- Scenario 3 (coast down with stop): The vehicle coasts down and stops at the intersection (red solid line);
- Scenario 4 (coast down without stop or glide): The vehicle slows down and passes through the intersection without stopping, and then speeds up to its initial speed (yellow dashed line).

B. Human Factor in Ecodriving Technology

Some of the current connected ecodriving technologies are based on the assumption that the driver is able to follow the instruction precisely, which is actually impossible in most cases. In our previous study, the fuel savings from the EAD system for an ICE vehicle traveling along an actuated signalized corridor was found to reach 10% in numerical simulation [21], but it was only 2% in real-world test driving [22]. The difference in fuel savings benefit is at least partially due to the imperfection of the human driver trying to follow the recommended speed profile. In this study, we define "human driver error" as the error when driver is trying to follow the suggested optimal driving strategy (e.g., optimal speed), which is elaborated in the following section. There are also some efforts that explicitly investigated the energy impact of human driver error on ecodriving systems. In [23], a proportional-integral-derivative (PID) function is used to model driver behavior in response to the speed guidance. The simulation results show 4% of energy savings as compared to the scenario without considering driver behavior. One possible

issue in applying such model is the difficulty in identifying the appropriate gains for the proportional, integral, and derivative components that reflect different driving habits. In addition, this PID model is not good at considering the expected human driver error in future time steps and therefore no optimization is conducted according to such error.

There are some existing results on stochastic model predictive control (SMPC), but most of them are on linear systems [29]–[31]. For example, in [29], a stochastic model predictive control method is used for hybrid electric vehicle (HEV) energy management. It treats human error as a stochastic process, models human error with Markov chains, applies a linear stochastic model predictive control to HEV energy management, and simplifies the computation burden with scenario based algorithms. But this study does not consider the nonlinear dynamics of vehicles, which is very important to reduce energy consumption of the vehicles. There is very limited study on nonlinear stochastic model predictive control. The stability of nonlinear SMPC using Markov chain Monte Carlo optimization is discussed in [32]. The nonlinear systems with Markov switching properties is investigated in [33]. But neither of them deal with the computational issues.

To address these issues, we propose a Markov chain based driving error estimation model based on a nonlinear longitudinal dynamics of vehicles. The error estimation model can adapt to the changing driving behavior and also estimate the driving error in multiple time steps ahead. The nonlinear longitudinal dynamics of vehicles can model the movement of vehicles in a more precise way so that the results can be more practical. In addition, scenario based SMPC as described in [29] is adopted to address the high computational cost issue. We select the total number of scenarios to achieve a balance between the optimality and the computational overhead. Moreover, the approach in this paper can also be classified as human-in-loop semi-autonomous systems. Nunes *et al.* [34] gave a comprehensive overview of human-in-loop cyber-physical systems. Shia *et al.* [35] developed a semi-autonomous vehicular control method for threat assessment when correcting the human inputs is necessary. In [36], semi-autonomous vehicle control is considered for road departure and obstacle avoidance using a driver steering model. In this paper, we consider and model human errors as Markovian processes. More details are given in the following sections.

C. Connected Ecodriving Technology for EVs

While there has been much recent research on developing EAD systems for ICE vehicles, very little has been developed specifically for EVs. A dynamic programming (DP) based EAD system is developed for EVs along signalized arterials [24]. The proposed model was tested in the simulation with very limited signal phase conditions. Zhang and Yao [25] developed an EAD system for EVs based on their own EV energy consumption estimation model. The system evaluation was conducted in a simulation environment under four simple scenarios with different signal phases. To the best of our knowledge, there has been little research that investigates ecodriving systems for EVs based on real-world driving data. There has been no effort to account for human driver error in ecodriving technology for EVs either. This study aims to fill these research gaps.

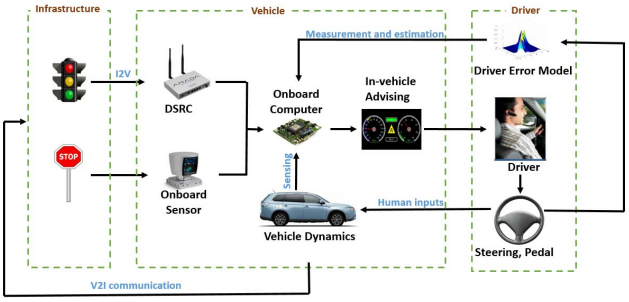

Fig. 2. A driver-vehicle-infrastructure cooperative framework for energy efficient driving.

III. Methodology

There are a variety of factors that influence the energy consumption of vehicles, which can be mainly classified into the following categories:

- *Vehicle-related:* Many vehicle-related factors could influence the energy consumption, such as powertrain type (i.e., ICE or EV), powertrain efficiency, vehicle mass, etc.
- *Driver-related:* Driving behavior is the major driver-related factor for vehicle energy consumption. For example, aggressive acceleration and deceleration causes additional energy consumption as compared to normal driving.
- *Infrastructure-related:* Traffic signal is one major type of traffic infrastructure in urban areas. It influences vehicle energy consumption due to stop and idle at signalized intersections.

In a driver-vehicle-infrastructure cooperation (DVIC) system (see Fig.2), the energy efficiency of EVs can be minimized by considering all the factors together in a connected vehicle environment. In the connected vehicle environment, a vehicle equipped with wireless communication devices can share its location, speed, heading, and many other data in real time with nearby equipped vehicles and the surrounding equipped infrastructure. Therefore, in the designed cooperative system, the vehicle and the infrastructure are tightly integrated by taking advantage of advanced wireless communications, high accuracy positioning, and on-board sensing technology. In addition, the impact of driving behavior is also integrated into the framework by modeling and estimating human driver error introduced into the control loop. In the designed cooperative system, the interaction between any two components (e.g., between infrastructure and vehicle) are bidirectional. For example, a vehicle can adjust its speed according to SPaT of the upcoming traffic signal. The traffic signal is also able to adjust its SPaT according to the vehicle states at the intersection (e.g., as in traffic signal priority).

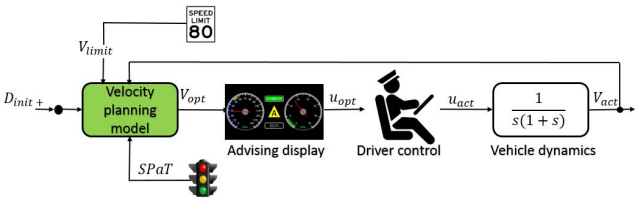

Fig. 3. Control flowchart of EAD system without considering driver error.

A. Connected Ecodriving Without Considering Driver Error

In this work, EAD systems are designed for EVs to achieve the most energy-efficient driving at signalized intersections. As a baseline for comparison, an EAD system without considering human driver error is designed according to Fig. 3. The vehicle trajectory planning algorithm (VTPA) generates an optimal speed profile based on real-time SPaT information. The optimal speed profile is advised to the human driver through the in-vehicle display, and the human driver controls the vehicle's longitudinal speed through the gas pedal and brake.

As explained in Fig.1, there are different passing scenarios for the vehicle to pass through a signalized intersection. Among all the possible speed profiles with which the vehicle can safely travel through the intersection, the vehicle trajectory planning algorithm (VTPA) will choose the one that minimizes tractive power requirements, and thus energy consumption of the EV(by assuming the motor efficiency and other loss are not dependent on vehicle dynamics). For a given passing scenario, the speed profile for approaching and departing the intersection is calculated using the distance to intersection d, desired time-to-arrival T, and vehicle speed $v_r(t_0)$ at current time t_0 (we suppose $t_0 = 0$ when calculating reference speed), based on the trigonometric model developed in our previous work [26], [37]. The reference speed of the vehicle $v_r(t)$ at time t for the speed-up scenario (Vehicle 2 in Fig. 1) is shown below as an example and those for other scenarios are put in the appendix:

$$v_r(t) = \begin{cases} v_h-(v_h-v(0))\cos(mt), & t\in\left[0,\frac{\pi}{2m}\right), \\ v_h-(v_h-v(0))\frac{m}{n} & \\ \quad \cos\left[n\left(t-\frac{\pi}{2m}+\frac{\pi}{2n}\right)\right], & t\in\left[\frac{\pi}{2m},\frac{\pi}{2m}+\frac{\pi}{2n}\right), \\ v_h+(v_h-v(0))\frac{m}{n}, & t\in\left[\frac{\pi}{2m}+\frac{\pi}{2n},\frac{d}{v_h}\right), \\ v_h-(v_h-v(0))\frac{m}{n} & \\ \quad \cos\left[n(t-\frac{d}{v_h}+\frac{\pi}{n})\right] & t\in\left[\frac{d}{v_h},\frac{d}{v_h}+\frac{\pi}{2n}\right), \\ v_h-(v_h-v(0))\cos & \\ \quad \left[n\left(t-\frac{d}{v_h}-\frac{\pi}{2m}+\frac{\pi}{2n}\right)\right], & t\in\left[\frac{d}{v_h}+\frac{\pi}{2n},\frac{\pi}{2m}+\frac{\pi}{2n}+\frac{d}{v_h}\right), \\ v(0), & t\in\left[\frac{\pi}{2m}+\frac{\pi}{2n}+\frac{d}{v_h},+\infty\right), \end{cases} \tag{1}$$

where $v_h = d/T$, $m > 0$ is the maximum value that satisfies

$$\begin{cases} m\cdot(v_h-v(0)) \le a_M \\ m^2\cdot(v_h-v(0)) \le du_M \\ m\cdot\left[m\left(\frac{dm}{v_h}-\frac{\pi}{2}\right)+\sqrt{m^2\left(\frac{dm}{v_h}-\frac{\pi}{2}\right)^2-4m^2\left(\frac{\pi}{2}-1\right)}\right] \\ \quad \cdot(v_h-v(0)) \le 2du_M \\ m \ge \frac{v_h}{d}\left(2\sqrt{\frac{\pi}{2}-1}+\frac{\pi}{2}\right) \text{ or } 0 < m \le \frac{v_h}{d}\left(\frac{\pi}{2}-2\sqrt{\frac{\pi}{2}-1}\right) \end{cases} \tag{2}$$

and

$$n = \frac{1}{2}\cdot\left[m\left(\frac{dm}{v_h}-\frac{\pi}{2}\right)+\sqrt{m^2\left(\frac{dm}{v_h}-\frac{\pi}{2}\right)^2-4m^2\left(\frac{\pi}{2}-1\right)}\right] \tag{3}$$

Here, parameters m and n determine the shape of the speed profile. They are also the dominant variables to control the energy efficiency of the acceleration and deceleration process. In [37], results indicated that if m and n satisfy Eq. (2) and (3), then the tractive power (of a generic vehicle model) would be minimized without compromising the driving comfort (constrained by the maximum jerk, du_M, in this study) and acceleration/deceleration capability (i.e., a_M and d_M). This trigonometric model was tested on ICE vehicles in our previous work which showed 10-15% fuel savings. In this study, a similar model is designed and tested on EVs to improve their energy efficiency by recommending smooth and energy-efficient speed profile at intersections.

B. Driver Error Modeling With Markov Chain Model

A nonlinear vehicle longitudinal dynamics model [27] is adopted in this work:

$$\dot{x}(t) = v(t), \tag{4a}$$

$$\dot{v}(t) = -\frac{1}{M}C_D\rho_a A_v v(t)^2 - \mu g - g\theta + u_f(t), \tag{4b}$$

$$u_f(t) = u(t) + w(t) \tag{4c}$$

where $x(t)$ is the vehicle's position; $v(t)$ is the velocity; $M = 1266$kg is the vehicle mass; θ is the road gradient ($\theta = 0$ in this work); g is the acceleration of gravity (i.e., 9.8 m/s^2); $u_f(t)$ is the braking or traction force per unit mass (i.e., the acceleration/deceleration generated from vehicle propulsion) and is considered as the sum of actual vehicle control; $u(t)$ is the optimal tractive force per unit mass suggested by the driving assistance system; $w(t)$ is the error (m/s^2) injected by the human when trying to follow the advised u; $C_D = 0.32$ is the drag coefficient; $\rho_a = 1.184$kg/m^3 is the air density; $A_v = 2.5$m^2 is the frontal area of the vehicle; and $\mu = 0.015$ is the rolling friction coefficient. The values of C_D, ρ_a, A_v, and μ can be found in [27].

The driver error in this study is defined as the difference between the actual tractive force per unit mass (resulted by human driver through gas paddle) and the optimal tractive force per unit distance calculated by the VTPA model.

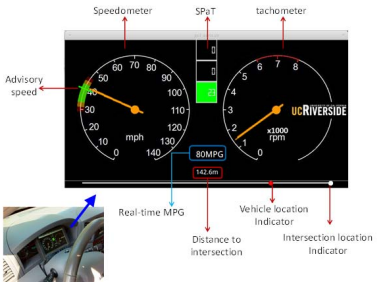

Fig. 4. HMI interface for in-vehicle advising.

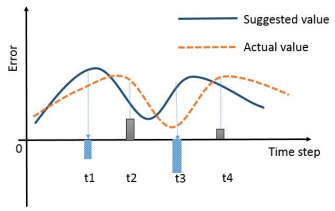

Fig. 5. Driver error calculation.

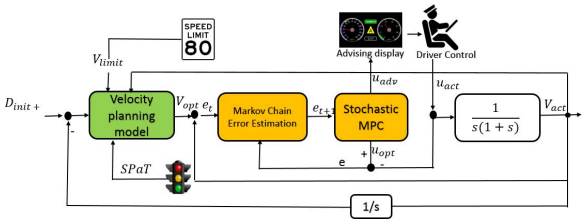

Fig. 6. Flowchart of EAD system considering driver error.

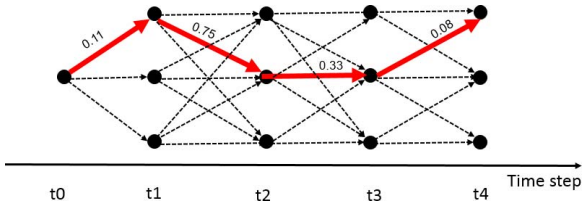

Fig. 7. Example scenario tree.

And it is generated by human drivers when trying to follow the advised speed displaying on the in-vehicle human-machine interface (HMI) as shown in Fig.4. Fig.5 provides an example on how to obtain the error from the real-world driving data.

To investigate the human error in a formal way, the error is first discretized into a finite number of states N_e. When we look at the human error along the time step, it can be observed that the human error in the next time step only depends on the current error and it is driver specific. Inspired by this Markovian property, a Markov chain model is adopted for modeling the human driver error and it can help represent the stochastic behavior of the human driver while tracking the advised command from driving assistance system.

Now the driver error dynamics is modeled as a Markov chain with a transition probability matrix T_e where its elements τ_{ij} represents the probability of error state transition from state i to j, where $i,\ j \leq N_e$

$$T_e = \begin{bmatrix} \tau_{11} & \tau_{21} & \tau_{31} & \cdots & \tau_{N_e 1} \\ \tau_{12} & \tau_{22} & \tau_{32} & \cdots & \tau_{N_e 2} \\ \tau_{13} & \tau_{23} & \tau_{33} & \cdots & \tau_{N_e 3} \\ \vdots & \vdots & \vdots & \vdots & \vdots \\ \tau_{1N_e} & \tau_{2N_e} & \tau_{3N_e} & \cdots & \tau_{N_e N_e} \end{bmatrix} \tag{5}$$

The transition matrix is driver specific and can be obtained from the real-world driving data collected from driving with the designed driving assistance system..

C. Connected Ecodriving Considering Driver Error

By taking into account the abovementioned driver error, an EAD system considering driver error is proposed (see Fig.5). In this system, the designed VTPA is integrated with a stochastic model predictive control (SMPC) strategy to calculate the optimal advisory speed for EV drivers (see Figure 2) based on the estimated human driver error when following the advice, so that the resulting actual vehicle speed (with human inputs) is as close to the calculated optimal vehicle trajectory as possible. For each optimization time horizon, the future human error during that time horizon is estimated based on the probability transition matrix learned from the historical driving data. From a control system perspective, the human input error actually is regarded as a source of disturbances. The receding horizon property of SMPC allows the system to better handle predictable disturbances. The control system diagram is provided in Figure 6.

The above vehicle dynamics model described in eq. (4) needs to be discretized as follows when implementing SMPC:

$$x\left(t_0+(k+1)\,\Delta t\right) = x\left(t_0+k\Delta t\right) + v\left(t_0+k\Delta t\right)\Delta t, \tag{6a}$$

$$\begin{aligned} v\left(t_0+(k+1)\,\Delta t\right) = {} & v\left(t_0+k\Delta t\right) \\ & + \left(-\frac{1}{M}C_D\rho_a A_v v\left(t_0+k\Delta t\right)^2\right. \\ & \left. - \mu g - g\theta + u_f\left(t_0+k\Delta t\right)\right)\Delta t, \end{aligned} \tag{6b}$$

where t_0 is starting time, Δt is sampling period, and k is time step. For brevity, we denote $x\left(t_0+k\Delta t\right)$ as $x\left(k\right)$, $v\left(t_0+k\Delta t\right)$ as $v\left(k\right)$, and $u_f\left(t_0+k\Delta t\right)$ as $u_f\left(k\right)$ in the remaining of this work.

For each finite time horizon, different trajectory states may depend on different human error w at each time step. Therefore, SMPC is used to solve this optimization problem with the uncertainty of human error during each finite time horizon. A *scenario tree* is developed consisting of different paths from the root node to the leaf nodes. The *root node* is the current state of the error w and the *leaf nodes* are the states reached from the current state at the end of the time horizon l. A *scenario is* defined by a path from the *root node* to *leaf nodes* with different w values for each time step within that time horizon. For each possible scenario, p_s is defined as the probability of its occurrence which is evaluated by the product of the probability of all edges in the path. The number of the generated scenario trees are denoted as N_{mc}. Figure 7 provides an example of a scenario tree when N_{mc} is 3 and only 4 time steps in the horizon.

Algorithm 1 Monte Carlo method

Input: total number of sampling paths as N_{mc}, time horizon l

Output: human errors $w\,(t, N_s)$ at times $t = 1, 2, \cdots, l-1$ for scenarios $N_s = 1, 2, \cdots, N_{mc}$.

1. **for** $N_s = 1 : N_{mc}$
2. **for** $t = 1 : l - 1$
3. generate a random number $r\,(t) \sim U\,[0, 1]$
4. set $w\,(t, N_s)$ as the j^{th} entry in the error vector if $\sum_{k=1}^{j-1} T_e(w(t-1, N_s), k) < r\,(t) \leq \sum_{k=1}^{j} T_e(w(t, N_s), k)$
5. **End for**
6. **End for**

To obtain the Markov chains of human error on acceleration, we first obtain velocity data of human drivers from road test and the reference velocity data generated in Appendix. With these velocity data, the difference (i.e., error) between acceleration resulted from human driving and the reference are computed. Then, we discretize the error data into several levels, count the numbers of transitions between different levels at consecutive time steps and divide them by the number of all transitions to get the transition matrix T_e. After obtaining T_e, we generate the scenarios trees with Algorithm 1. For example, as seen in Fig.7, the initial error at $t0$ is known. Then the error at time $t1$ is generated obeying the probability determined by the transition matrix in (5). From the generated error at $t1$, the error at time $t2$ is also generated from the transition matrix in (5). So are the errors at $t3$ and $t4$. We repeat the process N_{mc} times, where $N_{mc} = 3$ in Figure 7. The probability of occurrence of example scenario path (with red solid arrow) is p=0.11×0.75×0.33×0.08=0.0022, where the numbers at the red arrow represent the probability of state transition of the Markov chain.

When the probability of each possible path is obtained, the cost function of SMPC is defined as the expected (or mean) square errors between the reference speed and the predicted speed over the time horizon as follows:

$$\boldsymbol{E}\,(\boldsymbol{v} - \boldsymbol{v}_r)^2 = \sum_{s=1}^{N_{mc}} p_s \sum_{K=t+1}^{t+l} [v\,(k) - v_r\,(k)]^2, \tag{7}$$

where $\boldsymbol{E}$ represents expectation, $\boldsymbol{v}$ and $\boldsymbol{v}_r$ represent the real speed and the reference speed of the vehicle while $v\,(k)$ and $v_r\,(k)$ represent the real speed and reference speed at time instance k, where v_r is determined in (1).

Therefore, the objective function is defined as the expected sum of squared differences between the modeled and reference velocities. We also consider box constraints for the velocities, acceleration/deceleration, and jerk values. In summary, the optimal control problem based on SMPC can be formulated as:

$$argmin_{u_f} \sum_{s=1}^{N_{mc}} p_s \sum_{K=t+1}^{t+l} [v\,(k) - v_r\,(k)]^2$$

subject to the discritized dynamics (6)

$$\begin{aligned} &v_m \leq v\,(k) \leq v_M, \\ &\left|u_f\,(k)\right| \leq a_M, \\ &\left|u_f\,(k+1) - u_f\,(k)\right| \leq du_M, \end{aligned}$$

where t is the current time; l is the optimization horizon; $v\,(\cdot)$ is the velocity computed by the SMPC; $v_r\,(\cdot)$ is the reference velocity in (1); v_m is the minimum allowable speed, which is set to 0 in this work; v_M is the maximum allowable speed (usually the speed limit); u_M is the maximum acceleration/deceleration constrained by the vehicle propulsion power (here we suppose $a_M = d_M$); and du_M is the user-defined maximum jerk (mainly for driving comfort). We use 1 second as the sampling period and the control horizon of the SMPC is tunable and will be discussed later. Note that as the dynamics in Eq. (4) are nonlinear, the optimization problem at every time step of the SMPC is non-convex.

It is also noted that the total number of scenario paths is N_e^l. For example, if there are 10 levels of human error ($N_e = 10$) and the length of horizon is 10 ($l = 10$), then the total number of scenario path would be 10^{10}. Henceforth, the increase of N_e and l would significantly increase the computational time. To make the solving of this optimization problem more computationally tractable, the Monte Carlo method is adopted to generate N_{mc} realizations of scenario paths, where N_{mc}, the total number of sampling paths, is determined by balancing the accuracy and computational efficiency. For each sampling path, the predicted human error at next time instance is generated obeying the probability distribution of the transition matrix of Markov chain. Note that in Step 2, to obtain a predicted human error following the probability distribution of the Markov chain, a random number is generated by using a uniform distribution. If the generated number is between the accumulative distributed function values of the $(j-1)$th and jth error level, then the jth error level as the predicted error. To solve the optimization problem in the SMPC framework, the MATLAB command *fmincon* is used.

IV. Real-World Driving Data Preparation

To fully investigate the performance of the proposed driver-in-the-loop connected ecodriving system by comparing with the existing systems, real-world driving data with the designed open-loop EAD assistance system without considering human driver error was collected. The field test was conducted at the Turner-Fairbank Highway Research Center (TFHRC) in McLean, Virginia using the Saxton Lab Intelligent Intersection, which offered a sheltered traffic environment where the connected Ecodriving prototype was able to be tested with minimal safety risk and without disrupting live traffic operations [37]. Figure 8 provides an overview of the field test site, specifying starting point where the vehicle began test runs from a stop and traveled westbound towards the intersection and relevant roadside infrastructure (including an Econolite 2070 controller, Windows PC to encode SPaT and MAP messages, and Arada Locomate DSRC Roadside Unit). The test zone covers a range from 190 meters to the east of the intersection to 116 meters to the west, which allows a

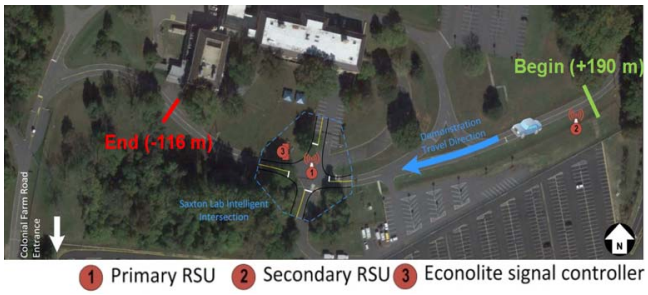

Fig. 8. Field study site in Turner Fairbank Highway Research Center in McLean, VA.

maximum traveling speed of up to 30 mph. The traffic signal controller was set up for fixed timed signal plan: 27 seconds of green, 3 seconds of yellow, followed by 30 seconds of red. The in-vehicle advising interface is shown in Fig.4.

In order to comprehensively investigate the energy benefits of the proposed system for EVs, we collected and processed real-world driving data in 3 different technological stages as elaborated in the following:

- Stage I: *Uninformed driving*. In this stage, the driver approached and traveled through the intersection in a normal fashion without guidance or automation, stopping as needed without any guidance. The vehicle was fully controlled by the human driver. This stage is used as lower bound performance technological stage.
- Stage II: *In-vehicle advising driving without considering driver error*. In this stage, the driver was assisted by an EAD system without considering driver error as described in Fig. 3. An enhanced dashboard presenting a recommended range of driving speed was provided (see Figure 4). This information could assist the driver to approach and depart from the intersection in an environment-friendly manner while obeying the traffic signal. This driving assistance system does not consider human driver error.
- Stage III: *In-vehicle advising driving with considering driver error.* At this stage, no real-world testing has been conducted due to the limited resources. Instead, we evaluated the performance of the designed EAD with the driver-in-the-loop system in a simulation environment developed in Matlab using data collected from the field testing of Stage II. The same VTPA model was used to calculate the optimal speed profile as part of the SMPC control model. More details about the simulation are given in the following sections.

To investigate different scenarios with respect to when a vehicle enters a signalized intersection and gets an average performance of the proposed system under various traffic conditions, the field experiment was designed to have the test vehicle approach the intersection at different time instances throughout the entire signal cycle (i.e., every 5 seconds in the 60-second cycle). We call these different entering cases as "*entry cases*" in the rest of this paper. Furthermore, the test vehicle approached the intersection at different operating speeds (i.e., 20 mph and 25 mph). Therefore, a test matrix was designed, consisting of the operating speed along the vertical axis, and the *entry case* across the horizontal access. In this matrix, there are a total of 12 *entry cases* $\times$ 2 speed levels $=$ 24 test cells. For Stage I and Stage II experiments, a total of four drivers were recruited to conduct test runs. Each driver completed each of the test cells in the test matrix. Therefore, a total of 24 test cells $\times$ 2 stages $\times$ 4 drivers $=$ 192 test runs were conducted. For each test run, data such as speed and distance to the stop bar were logged at 10 Hz and post-processed to determine energy consumption and other performance measures. It is noted that a hybrid vehicle (2012 Ford Escape) was used in the field study for the purpose of data collection. The energy consumption was estimated by the EV energy consumption model (see Section V) based on the collected driving speed trajectories for different cases. The proposed system is evaluated only on EV platform with a microscopic EV energy consumption model. The hybrid vehicle is only used for driving trajectories collection in the field test.

V. Simulation and Numerical Analysis

With the collected field driving data, additional simulation and numerical analysis are conducted to validate the performance of the proposed system.

A. EV Energy Consumption Estimation Model

Accurate estimation of EV energy consumption using real-world driving data (e.g., vehicle speed trajectory) is critical in evaluating the energy performance of different ecodriving technologies. In this study, a microscopic EV energy consumption estimation model developed in [25] considering the regenerative braking was adopted to calculate the EV energy consumption based on the vehicle speed profiles. This model is built based on the real-world EV driving data considering different EV driving mode, such as the acceleration mode, idling mode. For each driving mode, the real-world driving data includes the second-by-second vehicle speed and actual energy consumption. This model is used in this study to calculate the energy consumption of different EV driving trajectories. This model was designed for 4 different EV driving conditions: accelerating, decelerating, cruising and idling. The final model is presented as follows:

$$ECR = \begin{cases} e^{\left(\sum_{i=0}^{3}\sum_{j=0}^{3}(l_{i,j}\times v^i\times u_f^j)\right)} & u_f > 0 \\ e^{\left(\sum_{i=0}^{3}\sum_{j=0}^{3}(m_{i,j}\times v^i\times u_f^j)\right)} & u_f < 0 \\ e^{\left(\sum_{i=0}^{3}(n_i\times v^i)\right)} & u_f = 0,\ v \neq 0 \\ \overline{const} & u_f = 0,\ v = 0 \end{cases} \tag{8}$$

where *ECR* is energy consumption rate (Watt); $l_{i,j}$, $m_{i,j}$, and n_i are coefficients for ECR at speed power index $i (i = 0, 1, 2, 3)$ and acceleration power index j $(= 0, 1, 2, 3)$; v is instantaneous speed (km/h); u_f is instantaneous acceleration (m/s^2); $\overline{const}$ is the average energy consumption rate for idling. The coefficients in this model were obtained through training with real-world driving data and can be found in [25].

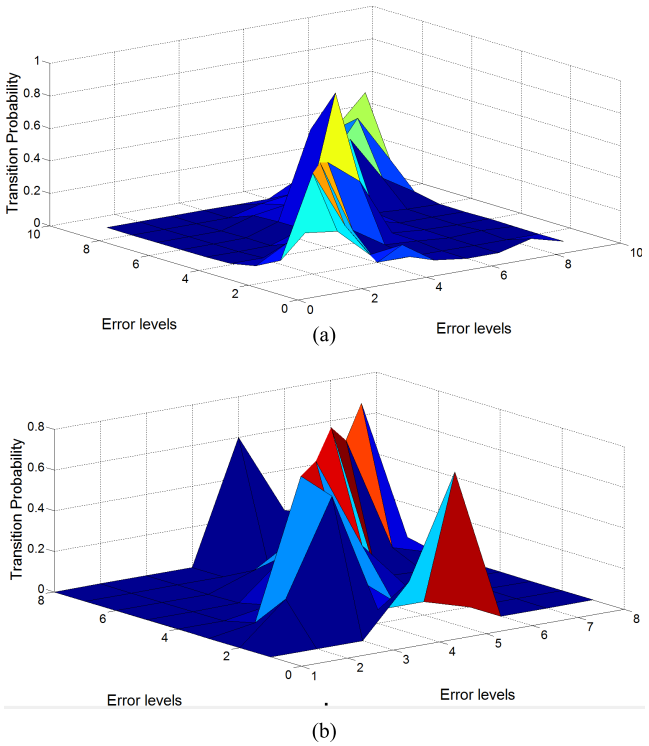

Fig. 9. 3-D plot of probability transition matrix. (a) Driver 1. (b) Driver 2.

B. Driver Error Estimation With Real-World Driving Data

As described in the previous section, the dynamics of human error is modeled as Markov chain. Now with the collected driving data, the probability transition matrix for each of these drivers can be built. In this study, the human error is discretized into 9 levels: −0.4, −0.3, −0.2, −0.1, 0, 0.1, 0.2, 0.3, 0.4. Please note the actual error value would not be those exact 9 values, but we use them to best approximate the actual value. For example, when the error is between −0.1 and 0.1 we use 0 as the estimated error value. In this work, the human driver error is extracted from the real-world with the method described in Fig.5 using the Stage II driving data. The probability transition matrix for each of the 4 drivers was built. For example, the transition matrix for driver 1 is given as follows and the 3-D plot is given in Fig. 9a.

$$\begin{bmatrix} \mathbf{0.33} & 0.31 & 0.13 & 0.15 & 0.03 & 0 & 0 & 0.05 & 0 \\ 0.12 & \mathbf{0.62} & 0.26 & 0 & 0 & 0 & 0 & 0 & 0 \\ 0.04 & 0.15 & \mathbf{0.60} & 0.15 & 0.03 & 0.02 & 0 & 0.01 & 0 \\ 0.01 & 0.01 & 0.06 & \mathbf{0.53} & 0.37 & 0.02 & 0 & 0 & 0 \\ 0 & 0 & 0 & 0.07 & \mathbf{0.87} & 0.05 & 0 & 0 & 0 \\ 0 & 0 & 0 & 0.07 & 0.60 & \mathbf{0.31} & 0.02 & 0 & 0 \\ 0 & 0 & 0 & 0.06 & 0.09 & 0.24 & \mathbf{0.42} & 0.15 & 0.03 \\ 0 & 0 & 0 & 0 & 0.05 & 0.08 & 0.21 & \mathbf{0.47} & 0.18 \\ 0 & 0 & 0 & 0 & 0 & 0 & 0.10 & 0.35 & \mathbf{0.55} \end{bmatrix}$$

As can be seen in the transition matrix, the diagonal entry of the matrix is the biggest value for each column. This implies the latency of human driving manipulation since the human error at the immediate next step is most likely to be within the same range of the current error level. It is also noticed that different drivers have different driving behavior or habit, which results in different transition matrix patterns that can be identified by comparing Fig.9a and Fig. 9b. For example, there are some off-diagonal peaks for Driver 2. The possible explanation of the off-diagonal is that driver 2 has some unique driving behavior, for example, driver 2 tends to give very aggressive acceleration when the driver notices the vehicle speed is blow certain speed level. The off diagonal could also be resulted from the error in the collected data. This could be a potential future research topic which is about identifying the relationship between different driving behaviors and the transition probability matrix patterns.

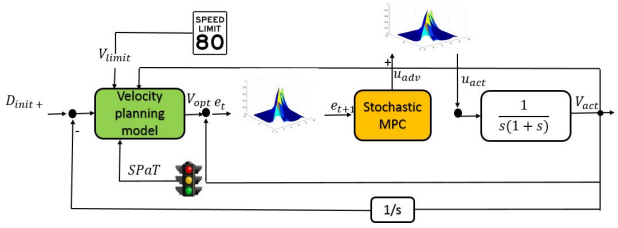

Fig. 10. Simulation framework.

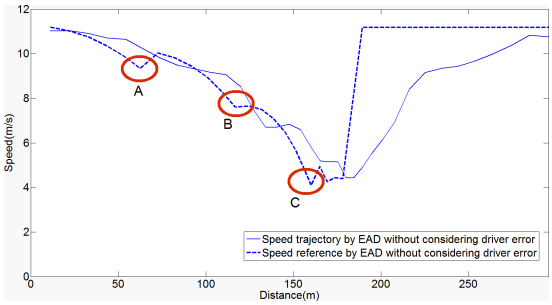

Fig. 11. Speed trajectory of EAD without considering driver error (real-world driving by driver 1 in *entry case* 11).

C. Simulation of EAD System Considering Driver Error

In this study, the EAD assistance system considering driver error was not implemented in filed driving but simulated with the real-world driving data collected from EAD assisted driving without considering driver error. In the simulation framework as shown in Fig.10, the built human error probability transition matrix is used in two places in the simulation for different purposes. One is used to estimate the human driver error that is input for the SMPC model. Another is used to replace the real human driver who adds in error when trying to follow the advised speed. These two matrices should be from the same driver and we assume the driving habit (represented by the error probability transition matrix) is not significantly changed during the simulation time.

To extensively evaluate the performance of EAD with driver-in-the-loop, the simulation is conducted using the field test driving data for every *entry case* described in the previous section (192 in total), so that the average performance can cover different driving conditions and different drivers. The vehicle speed trajectories obtained from the simulation are compared with that of real-world test driving. For example,

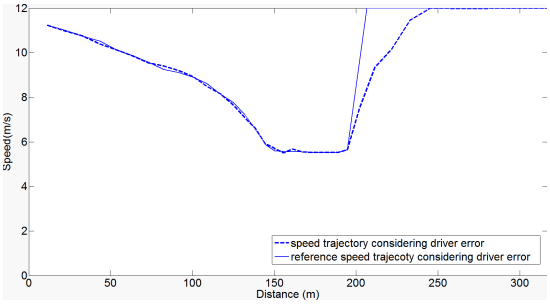

Fig. 12. Speed trajectory of EAD considering driver error(simulation driving).

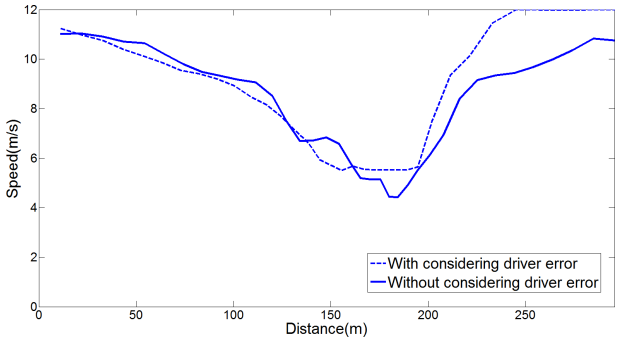

Fig. 13. Comparison of speed trajectories of two different EAD systems.

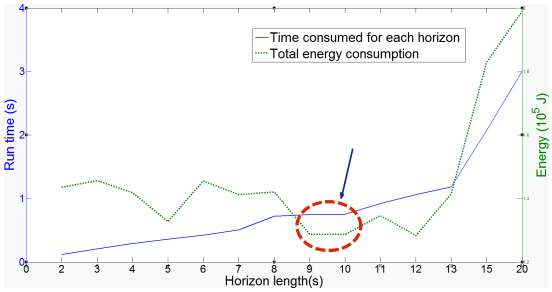

Fig. 14. Time and energy consumption by different horizon length.

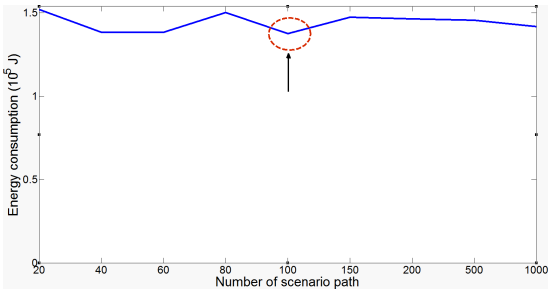

Fig. 15. Energy consumption by different number of scenario sampling size ($l = 10$).

Signal Phase	Entering Time(s)	Entry Case	Stage I	Stage II	Stage III
Green	27	1	3	3	4
	22	2	3	3	4
	17	3	3	3	4
	12	4	3	3	2
	7	5	1	1	1
	2	6	1	1	1
Red	27	7	1	1	1
	22	8	1	1	1
	17	9	1	1	1
	12	10	4	1	2
	7	11	3	4	4
	2	12	3	3	4

Scenario 1 Scenario 2 Scenario 3 Scenario 4

Fig. 16. *Passing scenario* at different *entry case*.

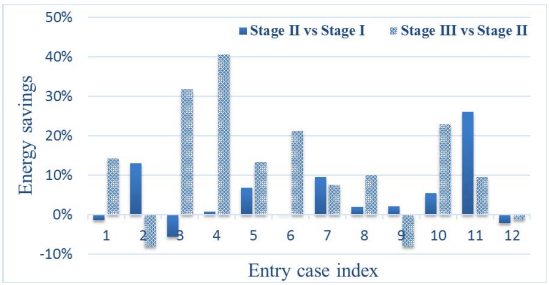

Fig. 17. Energy savings by different stages and *entry case* (driver 1).

Fig.11 provides the vehicle speed trajectory and its reference speed trajectory in *entry case* 11. As we can see in the figure, the reference speed is adjusted or recalculated for 3 times (marked by A, B, and C in the figure) due to the increased human driving following error. Although with the reference speed adjustment, the final driving speed trajectory is still away from the advised optimal speed due to the unavoidable human error. However, in Fig.12, we can see that the speed trajectory by EAD with driver-in-the-loop follows the referenced speed trajectory for most of the simulation time (using the same initial speed, initial position and entry time). It is also observed that the speed trajectory resulting from EAD with considering driver error is much smoother than that of EAD without (shown in Fig. 13), which could be another reason of energy saving that will be discussed in the following sections.

D. Real-Time Performance and Parameter Tuning

In the implementation of the proposed SMPC system, to ensure the real-time performance, the optimization of each time horizon should be finished within one-time step (e.g., 1s). In our study, the running time is recorded on the computing platform used for simulation (with Intel Core i7 3.4GHz, RAM 4G, and 64bit-Matlab 2012). Fig. 16 provides the time consumed for time horizon by different horizon length (for driver 1 and entry case 7, and the total number of sampling paths is 100). As we can see that, more than 1 second is consumed when the horizon length is longer than 10s, which means the real-time performance is ensured when horizon length is shorter than 10s. It is also noticed that the minimal energy consumption (marked in the Fig.14 with a circle) is identified around the horizon length 9 and 10. Therefore, the length of the receding horizon (l) in this study is set as 10.

In addition, another important parameter that can be tuned to maximize the performance of the SMPC based EAD with

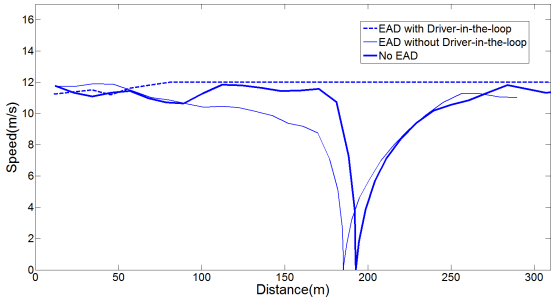

Fig. 18. Speed trajectory of EAD with/without driver-in-the-loop (for case 4, driver 1).

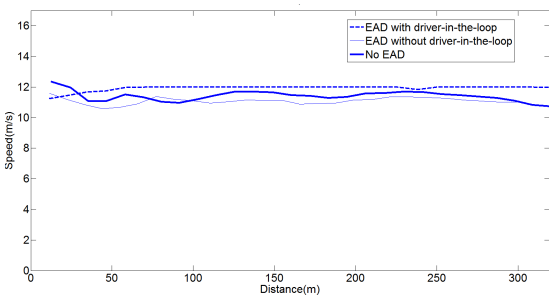

Fig. 19. Speed trajectory of EAD with/without driver-in-the-loop (for case 9, driver 1).

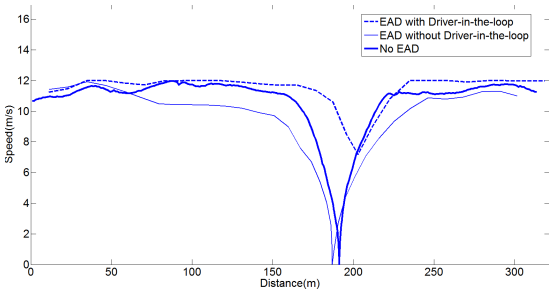

Fig. 20. Speed trajectory of EAD with/without driver-in-the-loop (for case 12, driver 1).

driver-in-the-loop, is the total number of sampled scenario paths (N_{mc}). Fig. 15 presents the energy consumption by different numbers of scenario path sampling size and it is observed that the increase of sampling size is not able to improve the performance (i.e., reduce energy consumption). A possible reason is that, the scenario path with very small probability is not likely to be sampled no matter how large the sample size is. Hence we set the sampling size (N_{mc}) is 100, which is marked by a circle in the figure.

E. Energy Savings Analysis

As described in Fig.1, there are 4 different *passing scenarios* for a vehicle passing through an intersection. Fig. 18 gives the passing scenarios (in different colors) resulting from different stages of technology (for driver 1 with 25 mph initial speed). It is observed in Fig.16 that for some *entry cases*, the passing scenario is changed due to the consideration of human driver error in the EAD system. For example, for entry case 1, the test scenario in EAD with considering driver error is 4 rather than 3 in EAD without considering driver error. It shows that a full stop at the intersection is avoided due to the technology improvement, which will potentially reduce the energy consumption.

TABLE I
SCENARIO-CHANGE ANALYSIS

Stage	Scenario Change	Energy savings		
		min	mean	max
II vs III	3-›2	19.1%	25.7%	40.5%
II vs III	3-›4	9.9%	18.9%	26.7%
II vs III	1-›1	-6.7%	1.3%	10.3%
II vs III	4-›4	-15.5%	1.9%	13.2%

TABLE II
AVERAGE ENERGY AND MOBILITY IMPROVEMENT

Stage	Energy benefit (Energy savings)		
	min	mean	max
III vs II	-8.9%	11.7%	40.5%
II vs I	-14.3%	12.1%	27%

As can be seen in Fig.17, the energy savings of Stage III comparing to Stage II is significantly different for different *entry case*. The largest energy saving occurs at the *entry case* 4 (40.5%) and the speed trajectories are shown in Fig.18. The energy saving is due to the passing scenario change from 3 to 2. The avoidance of stop-and-go maneuvers is the main reason of the energy benefit.

For the *entry case* 9, all the three stages result in *passing scenario 1*. Therefore, there would be no significant energy savings but even a smaller increase of energy consumption (-7.8 %) due to the stochastic property of the SMPC strategy. For the *entry case* 12, the energy saving (2.3%) is due to the reduction of acceleration comparing a full stop for Stage I or II. But this energy saving is much smaller comparing to the *entry case* 4 (see Fig.18) where the unnecessary deceleration and acceleration are completely avoided. In addition, the energy savings of Stage II comparing to Stage I are also given in Fig.17.

To obtain a statistical performance evaluation, the collected data of all the test driving and simulated driving (288 trips in total) are used to calculate the energy savings resulting from different stages of technologies. Table I gives the basic statistics of energy savings for different *passing scenario* changes. The change from 3 to 2 or 4 could result in the majority of energy savings due to the reduced unnecessary acceleration from low speed.

The overall average savings of Stage II vs. Stage I and Stage III vs Stage II are listed in Table II. The EAD system without considering driver error achieves 12.1% of energy savings comparing to the human driving without any EAD assistance. And the EAD assistance with considering driver error can achieve 11.7% of energy savings comparing to EAD system without. It shows that considering human driving errors

in driving assistance systems has great potential in improving the energy performance of connected ecodriving for electric vehicles.

VI. Conclusions and Future Work

In this study, a connected ecodriving system for energy-efficient driving considering human driver error is proposed under a driver-vehicle-infrastructure cooperation framework. The proposed system is evaluated with EV energy consumption models and compared with the conventional ecodriving system without considering driver error. Real-world driving data was collected and used to comprehensively evaluate system performance in terms of energy consumption. The simulation analysis shows that an average of 12% energy savings can be achieved by the proposed system that accounts for human driver error. The obvious limitation of this study is that it does not consider the impact of traffic conditions which are expected to degrade the energy saving performance of the proposed system. But the finding of this study will be used as the performance upper bound with no traffic impact. Future work will be focused on further evaluation of this proposed system with more real-world testing that considers different traffic conditions.

Appendix

Reference speed for coast-down-with-stop scenario (vehicle 3 in Fig. 1):

$$v_r(t)=\begin{cases} v_h-(v_h-v\,(0))\cdot\cos(mt), \\ \qquad t\in\left[0,\ \dfrac{\pi}{2m}\right) \\ v_h-(v_h-v\,(0))\cdot\dfrac{m}{n}\cdot\cos\left[n\cdot\left(t-\dfrac{\pi}{2m}+\dfrac{\pi}{2n}\right)\right], \\ \qquad t\in\left[\dfrac{\pi}{2m},\ \dfrac{\pi}{2m}+\dfrac{\pi}{2n}\right) \\ v_h+(v_h-v(0))\cdot\dfrac{m}{n}, \\ \qquad t\in\left[\dfrac{\pi}{2m}+\dfrac{\pi}{2n},\ g_s^2\right) \\ v_h-(v_h-v\,(0))\cdot\dfrac{m}{n}\cdot\cos\left[n\cdot\left(t-g_s^2+\dfrac{\pi}{n}\right)\right], \\ \qquad t\in\left[g_s^2,\ g_s^2+\dfrac{\pi}{2n}\right) \\ v_h-(v_h-v\,(0))\cdot\cos\left[m\cdot\left(t-g_s^2-\dfrac{\pi}{2m}-\dfrac{\pi}{2n}\right)\right], \\ \qquad t\in\left[g_s^2+\dfrac{\pi}{2n},\ g_s^2+\dfrac{\pi}{2m}+\dfrac{\pi}{2n}\right) \\ v\,(0), \\ \qquad t\in\left[g_s^2+\dfrac{\pi}{2m}+\dfrac{\pi}{2n},\ +\infty\right) \end{cases}$$

and,

$$m=\frac{\pi\cdot v_h}{d}$$

and $n=m$, $v_h=d/T$, and g_s^2 represents the start time of the second green window.

Reference speed for coast-down-without-stop scenario (vehicle 4 in Fig. 1):

$$v_r(t)=\begin{cases} v_h-(v_h-v\,(0))\cdot\cos(mt), \\ \qquad t\in\left[0,\ \dfrac{\pi}{2m}\right) \\ v_h-(v_h-v\,(0))\cdot\dfrac{m}{n}\cdot\cos\left[n\cdot\left(t-\dfrac{\pi}{2m}+\dfrac{\pi}{2n}\right)\right], \\ \qquad t\in\left[\dfrac{\pi}{2m},\ \dfrac{\pi}{2m}+\dfrac{\pi}{2n}\right) \\ v_h+(v_h-v(0))\cdot\dfrac{m}{n}, \\ \qquad t\in\left[\dfrac{\pi}{2m}+\dfrac{\pi}{2n},\ \dfrac{d_0}{v_h}\right) \\ v_h-(v_h-v\,(0))\cdot\dfrac{m}{n}\cdot\cos\left[n\cdot\left(t-\dfrac{d_0}{v_h}+\dfrac{\pi}{n}\right)\right], \\ \qquad t\in\left[\dfrac{d_0}{v_h},\ \dfrac{d_0}{v_h}+\dfrac{\pi}{2n}\right) \\ v_h-(v_h-v\,(0))\cdot\cos\left[m\cdot\left(t-\dfrac{d_0}{v_h}-\dfrac{\pi}{2m}-\dfrac{\pi}{2n}\right)\right], \\ \qquad t\in\left[\dfrac{d_0}{v_h}+\dfrac{\pi}{2n},\ \dfrac{d_0}{v_h}+\dfrac{\pi}{2m}+\dfrac{\pi}{2n}\right) \\ v\,(0), \\ \qquad t\in\left[\dfrac{d_0}{v_h}+\dfrac{\pi}{2m}+\dfrac{\pi}{2n},+\infty\right) \end{cases}$$

and m (>0) is chosen as the maximum that satisfies:

$$\begin{cases} m\cdot(v\,(0)-v_h)\le a_M \\ m^2\cdot(v\,(0)-v_h)\le du_M \\ m\cdot\left[m\left(\dfrac{dm}{v_h}-\dfrac{\pi}{2}\right)+\sqrt{m^2\left(\dfrac{dm}{v_h}-\dfrac{\pi}{2}\right)^2-4m^2\left(\dfrac{\pi}{2}-1\right)}\right] \\ \quad\cdot(v\,(0)-v_h)\le 2du_M \\ m\ge\dfrac{v_h}{d}\left(2\sqrt{\dfrac{\pi}{2}-1}+\dfrac{\pi}{2}\right)\ \ or\ \ 0<m\le\dfrac{v_h}{d}\left(\dfrac{\pi}{2}-2\sqrt{\dfrac{\pi}{2}-1}\right), \end{cases}$$

$v_h=d/T$, and

$$n=\frac{1}{2}\cdot\left[m\left(\frac{dm}{v_h}-\frac{\pi}{2}\right)+\sqrt{m^2\left(\frac{dm}{v_h}-\frac{\pi}{2}\right)^2-4m^2\left(\frac{\pi}{2}-1\right)}\right]. \tag{9}$$

References

[1] U.S. Energy Information Administration. (Mar. 2015). *Monthly Energy Review Table 2.1*. [Online]. Available: http://www.eia.gov/Energyexplained/?page=us_energy_transportation

[2] L. Hockstad, "Inventory of U.S. Greenhouse gas emissions and sinks: 1990–2014," U.S. Environ. Protection Agency, Washington, DC, USA, Final Rep. EPA 430-R-16-002, Apr. 2016.

[3] X. Qi, G. Wu, K. Boriboonsomsin, and M. J. Barth, "An on-line energy management strategy for plug-in hybrid electric vehicles using an Estimation Distribution Algorithm," in *Proc. IEEE 17th Int. Conf. Intell. Transp. Syst. (ITSC)*, vol. 1, Oct. 2014, pp. 2480–2485, doi: 10.1109/ITSC.2014.6958087.

[4] X. Qi, G. Wu, K. Boriboonsomsin, M. J. Barth, and J. Gonder, "Data-driven reinforcement learning–based real-time energy management system for plug-in hybrid electric vehicles," *Transp. Res. Rec., J. Transp. Res. Board*, vol. 2572, pp. 1–8, Aug. 2016, doi: 10.3141/2572-01.

[5] X. Qi, G. Wu, K. Boriboonsomsin, and M. J. Barth, "A novel blended real-time energy management strategy for plug-in hybrid electric vehicle commute trips," in *Proc. IEEE 18th Int. Conf. Intell. Transp. Syst.*, Las Palmas, Spain, Sep. 2015, pp. 1002–1007.

[6] D. Schrank, B. Eisele, T. Lomax, and J. Bak. (2015). *Urban Mobility Scorecard*. [Online]. Available: http://d2dtl5nnlpfr0r.cloudfront.net/tti.tamu.edu/documents/mobility-scorecard-2015.pdf

[7] M. Barth, G. Wu, H. Xia, Q. Jin, and K. Boriboonsomsin, "AERIS field study application: Eco-approach to signalized intersections," U.S. Dept. Transp., Washington, DC, USA, Final Rep. FHWA-JPO-12-063, Sep. 2012.

[8] Q. Jin, G. Wu, K. Boriboonsomsin, and M. J. Barth, "Energy and emissions benefits of a real-time driving speed advisory system for heavy-duty trucks," in *Proc. Annu. Meeting Transp. Res. Board*, Washington, DC, USA, 2016, pp. 111–119.

[9] M. Faraj and O. Basir, "Range anxiety reduction in battery-powered vehicles," in *Proc. IEEE Transp. Electrific. Conf. Expo (ITEC)*, Dearborn, MI, USA, Jun. 2016, pp. 1–6.

[10] J. Axsen, K. S. Kurani, and A. Burke, "Are batteries ready for plug-in hybrid buyers?" *Transp. Policy*, vol. 17, no. 3, pp. 173–182, 2010.

[11] K. Morrowa, D. Karnerb, and J. Francfortc, "Advanced vehicle testing activity. Plug-in hybrid electric vehicle charging infrastructure review," U.S. Dept. Energy's Vehicle Technol. Program, Battelle Energy Alliance, Washington, DC, USA, Final Rep. INL/EXT-08-15058, 2008.

[12] European Commission (EC). *eCoMove—Cooperative Mobility Systems and Services for Energy Efficiency*. Accessed: Jan. 23, 2017. [Online]. Available: http://www.ecomove-project.eu/

[13] European Union (EU). *Compass4D—One Step Closer to C-ITS Deployment in Cities*. Accessed: Jan. 23, 2017. [Online]. Available: http://www.compass4d.eu/

[14] U.S. Dept. Transp. (USDOT). *Applications for the Environment: Real-Time Information Synthesis (AERIS)*. Accessed: Jan. 23, 2017. [Online]. Available: http://www.its.dot.gov/aeris/

[15] *AERIS Concept of Operations and Modeling Workshop*, U.S. Dept. Transp., Washington, DC, USA, Mar. 2013.

[16] B. Asadi and A. Vahidi, "Predictive cruise control: Utilizing upcoming traffic signal information for improving fuel economy and reducing trip time," *IEEE Trans. Control Syst. Technol.*, vol. 19, no. 3, pp. 707–714, May 2011.

[17] W. Li, G. Wu, M. Barth, and Y. Zhang, "Safety, mobility and environmental sustainability of eco-approach and departure application at signalized intersections: A simulation study," in *Proc. IEEE Intell. Vehicles Symp. (IV)*, Gothenburg, Sweden, Jun. 2016, pp. 1109–1114.

[18] M. Seredynski, B. Dorronsoro, and D. Khadraoui, "Comparison of green light optimal speed advisory approaches," in *Proc. 16th IEEE Conf. Intell. Transp. Syst. (ITSC)*, Oct. 2013, pp. 2187–2192.

[19] R. Kamalanathsharma and H. Rakha, "Agent-based simulation of ecospeed-controlled vehicles at signalized intersections," *Transp. Res. Rec., J. Transp. Res. Rec.*, vol. 2427, pp. 1–12, Dec. 2014.

[20] Z. Chen, Y. Zhang, J. Lv, and Y. Zou, "Model for optimization of ecodriving at signalized intersections," *Transp. Res. Rec., J. Transp. Res. Rec.*, vol. 2427, pp. 54–62, Dec. 2014.

[21] P. Hao, G. Wu, K. Boriboonsomsin, and M. J. Barth, "Developing a framework of eco-approach and departure application for actuated signal control," in *Proc. IEEE Intell. Vehicles Symp. (IV)*, Jun. 2015, pp. 796–801.

[22] P. Hao, G. Wu, K. Boriboonsomsin, and M. J. Barth, "Eco-approach and departure (EAD) application for actuated signals in real-world traffic," in *Proc. 96th Annu. Meeting Transp. Res. Board*, Washington, DC, USA, 2017, pp. 92–107.

[23] X. Xiang, K. Zhou, W.-B. Zhang, W. Qin, and Q. Mao, "A closed-loop speed advisory model with driver's behavior adaptability for eco-driving," *IEEE Trans. Intell. Transp. Syst.*, vol. 16, no. 6, pp. 3313–3324, Dec. 2015.

[24] M. Miyatake, M. Kuriyama, and Y. Takeda, "Theoretical study on eco-driving technique for an electric vehicle considering traffic signals," in *Proc. IEEE 9th Int. Conf. Power Electron. Drive Syst. (PEDS)*, Singapore, Dec. 2011, pp. 733–738.

[25] R. Zhang and E. Yao, "Eco-driving at signalised intersections for electric vehicles," *IET Intell. Transp. Syst.*, vol. 9, no. 5, pp. 488–497, 2015.

[26] M. Barth, S. Mandava, K. Boriboonsomsin, and H. Xia, "Dynamic ECO-driving for arterial corridors," in *Proc. IEEE Forum Integr. Sustain. Transp. Syst.*, Vienna, Austria, Jun./Jul. 2011, pp. 182–188.

[27] M. A. S. Kamal, M. Mukai, J. Murata, and T. Kawabe, "Model predictive control of vehicles on urban roads for improved fuel economy," *IEEE Trans. Control Syst. Technol.*, vol. 21, no. 3, pp. 831–841, May 2013.

[28] R. H. Byrd, M. E. Hribar, and J. Nocedal, "An interior point algorithm for large-scale nonlinear programming," *SIAM J. Optim.*, vol. 9, no. 4, pp. 877–900, 1999.

[29] S. Di Cairano, D. Bernardini, A. Bemporad, and I. V. Kolmanovsky, "Stochastic MPC with learning for driver-predictive vehicle control and its application to HEV energy management," *IEEE Trans. Control Syst. Technol.*, vol. 22, no. 3, pp. 1018–1031, May 2014.

[30] D. Bernardini and A. Bemporad, "Stabilizing model predictive control of stochastic constrained linear systems," *IEEE Trans. Autom. Control*, vol. 57, no. 6, pp. 1468–1480, Jun. 2012.

[31] P. D. Couchman, M. Cannon, and B. Kouvaritakis, "Stochastic MPC with inequality stability constraints," *Automatica*, vol. 42, no. 12, pp. 2169–2174, Dec. 2006.

[32] E. Siva, P. Goulart, J. Maciejowski, and N. Kantas, "Stability of model predictive control using Markov Chain Monte Carlo optimisation," in *Proc. Eur. Control Conf. (ECC)*, Budapest, Hungary, Aug. 2009, pp. 2851–2856.

[33] P. Patrinos, P. Sopasakis, H. Sarmiveis, and A. Bemporad, "Stochastic model predictive control for constrained discrete-time Markovian switching systems," *Automatica*, vol. 50, pp. 2504–2514, Oct. 2014.

[34] D. S. Nunes, P. Zhang, and J. S. Silva, "A survey on human-in-the-loop applications towards an Internet of all," *IEEE Commun. Surveys Tuts.*, vol. 17, no. 2, pp. 944–965, 2nd Quart., 2015.

[35] V. A. Shia *et al.*, "Semiautonomous vehicular control using driver modeling," *IEEE Trans. Intell. Transp. Syst.*, vol. 15, no. 6, pp. 2696–2709, Dec. 2014.

[36] G. Andrew, M. Ali, Y. Gao, J. Hedrick, and F. Borrelli, "Semi-autonomous vehicle control for road departure and obstacle avoidance," in *Proc. IFAC Control Transp. Syst.*, 2012, pp. 1–6.

[37] O. D. Altan, G. Wu, M. J. Barth, K. Boriboonsomsin, and J. A. Stark, "GlidePath: Eco-friendly automated approach and departure at signalized intersections," *IEEE Trans. Intell. Vehicles*, vol. 2, no. 4, pp. 266–277, Dec. 2017.

Xuewei Qi (M'13) received the M.S. degree in engineering from The University of Georgia, Athens, in 2013, and the Ph.D. degree in electrical and computer engineering from University of California at Riverside (UC Riverside), Riverside, in 2016. He was with the Center for Environmental Research and Technology, College of Engineering, UC Riverside, when this study was carried out. His recent research focuses on deep learning-based perception and motion planning for autonomous vehicles, computer vision, and camera and LIDAR sensor fusion. He is currently an AI Scientist in autonomous vehicle technology with General Motors. He is also serving as a Committee Member of the Alternative Transportation Fuels and Technologies Standing Committee (ADC80) and the Artificial Intelligence and Advanced Computing Standing Committee (ABJ70) of the U.S. Transportation Research Board. He is also member of the IEEE Intelligent Transportation System Society, the IEEE Computational Intelligence Society, the IEEE Internet of Things Society, and the Institute of Transportation Engineers. He is a Guest Editor of IEEE SENSORS JOURNAL.

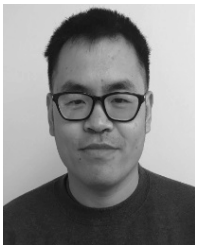

Peng Wang received the B.S. degree in mathematics from Shandong University, the M.S. degree in control science and engineering from Shanghai Jiao Tong University, and the Ph.D. degree in electrical engineering from University of California, Riverside. His recent research interests include distributed optimization and control in large-scale systems.

Guoyuan Wu (M'09–SM'15) received the Ph.D. degree in mechanical engineering from University of California at Berkeley, Berkeley, in 2010. From 2005 to 2010, he was a Graduate Student Researcher with the California Partners for Advanced Transportation Technology. He currently holds an assistant research engineer position with the Center for Environmental Research and Technology, Transportation Systems Research Group, Bourns College of Engineering, University of California at Riverside. His research focuses on intelligent and sustainable transportation system technologies, optimization and control of transportation systems, and traffic simulation. He is also a member of the Vehicle-Highway Automation Committee (AHB30) of the Transportation Research Board, the Institute of Transportation Engineers, and the Chinese Overseas Transportation Association.

Kanok Boriboonsomsin (M'14) received the Ph.D. degree in transportation engineering from University of Mississippi, Oxford, MS, USA, in 2004. He is currently an Associate Research Engineer with the Center for Environmental Research and Technology, College of Engineering, University of California at Riverside, Riverside. His research interests include sustainable transportation systems and technologies, intelligent transportation systems, traffic simulation, traffic operations, transportation modeling, vehicle emissions modeling, and vehicle activity analysis. He is a member of the Transportation and Air Quality Standing Committee of Transportation Research Board, the Institute of Transportation Engineers, and the IEEE ITSS. He serves as an Associate Editor for *IEEE Intelligent Transportation Systems Magazine*.

Matthew J. Barth (M'90–SM'00–F'14) received the B.S. degree in electrical engineering/computer science from University of Colorado, Boulder, CO, USA, in 1984, and the M.S. and Ph.D. degrees in electrical and computer engineering from University of California, Santa Barbara, CA, USA, in 1986 and 1990, respectively. He is currently a Yeager Families Professor with the Department of Electrical Engineering and the Director of the Center for Environmental Research and Technology, University of California, Riverside, CA, USA. His research interests include intelligent transportation systems, transportation/emissions modeling, vehicle activity analysis, electric vehicle technology, robotics, and advanced sensing and control. He was the President of the IEEE Intelligent Transportation System Society from 2014 to 2015. He serves as a Senior Editor for IEEE TRANSACTIONS ON INTELLIGENT VEHICLES and IEEE TRANSACTIONS ON INTELLIGENT TRANSPORTATION SYSTEMS. He is also active in several committees of the Transportation Research Board, including the Intelligent Transportation Systems Committee.